Compact Wide Single-/Dual- Band Bandpass Filter with Equal Inductance Configuration in Thin Film IPD Technology

Zhi-Hao Liu[1], Bao-Guang Liu[1], Chong-Hu Cheng[1], Yong Cheng[1] ✉
1 The College of Electronic and Optical Engineering & College of Flexible Electronics (Future Technology), Nanjing University of Post and Telecommunications, Nanjing 210046, China. (e-mail: lzh_njupt@163.com; chengy@njupt.edu.cn)

In this paper, based on thin film integrated passive device (TF-IPD) technology, compact ultra-wideband (UWB) bandpass filter (BPF) and dual-band bandpass filter (DBBPF) with equal inductance configuration are proposed. The configuration of equal inductance in a circuit contributes to reducing variables, simplifying the physical structure, and shortening the debugging time in the TF-IPD design process. Despite all the inductors being equal in value, wide passband can still be achieved. The measured results show that the center frequency of UBW BPF is 11.43 GHz, the 3-dB fractional bandwidth (FBW) is 133% (3.87 GHz-18.99 GHz). And the 3-dB FBWs of DBBPF centered at 6.5 GHz and 16.2 GHz are 92% (3.51-9.49 GHz) and 35% (13.33-18.98 GHz), respectively. The stopband of UBW BPF and DBBPF can be extended to 47.7 GHz and 44.8 GHz in sizes of 321 um × 856 um and 235 um × 846 um, respectively (excluding measuring pads).

Introduction: The filter, being an essential component in communication systems, has garnered significant attention. With the advancement of process, filters have become increasingly smaller in size. Currently, various semiconductor technologies, such as CMOS[1]–[4], TF-IPD (GaAs-IPD[5], [6], Si-IPD[7], Glass-IPD[8]), LTCC[9]–[11], can achieve extremely narrow width and spacing. Filters designed using semiconductor technology exhibit characteristics such as miniaturization, seamless integration, and high stability. However, existing filters[1]–[11] developed through semiconductor technology often feature complex structures with numerous components. And the distribution effects of the lumped components gradually increase at higher frequency - especially in terms of inductor. The physical structure of inductor exhibits a complex equivalent circuit[12], [13] at high frequency. When there are many different inductors in the circuit, it will increase the complexity of debugging and physical structure.

In this paper, based on TF-IPD technology, compact ultra-wideband (UWB) bandpass filter (BPF) and dual-band bandpass filter (DBBPF) with equal inductance configuration are proposed. The configuration of equal inductance in a circuit contributes to reducing variables, simplifying the physical structure, and shortening debugging time in the TF-IPD design process. The circuit of both filters is a lumped dual-loop circuit. And the circuit has a reduced number of components and variables, containing 9 components in which there are 5 variables. Although all inductors in the circuit are the same, it can still achieve wide passband. The measured results show that the UWB BPF has a center frequency of 11.43 GHz and a 3-dB FBW of 133%. And the 3-dB FBWs of DBBPF centered at 6.5 GHz and 16.2 GHz are 92% and 35%. The stopband of UWB BPF and DBBPF can be extended to 47.7 GHz and 44.8 GHz in sizes of 321 um × 856 um and 235 um × 846 um, respectively (excluding measuring pads).

Analysis and design: The circuit of both filters is a lumped dual-loop circuit, shown in Fig.1 (a). The circuit consists of four identical inductors L_1, two capacitors C_2, two capacitors C_3, and one C_1, where there is a coupling coefficient M between each of the two inductors. The topology has only 5 variables, and the four inductors are coupled in pairs, so it has the characteristics of simple design and compact structure. According to the different component values in the topology, the proposed filters can be designed into UWB BPF and DBBPF. This topology is analyzed in the following, and based on this topology, UWB BPF and DBBPF are designed and implemented by IPD process.

Since the circuit is not symmetrical, the 2-port circuit is converted into 4-port circuit, and it analyzed by the even- and odd- mode analytical method[14]. The even- and odd-mode equivalent circuits of the 4-port circuit are shown in Fig. 1 (b) and Fig.1 (c). And the ABCD

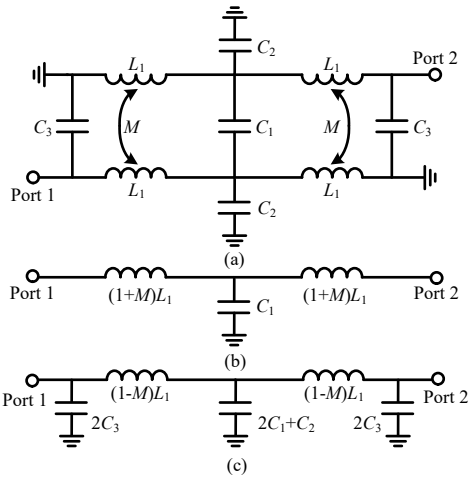

Fig. 1 *(a) The circuit of the proposed filters. (b) The even-mode equivalent circuit of 4-port circuit. (c) The odd-mode equivalent circuit of 4-port circuit.*

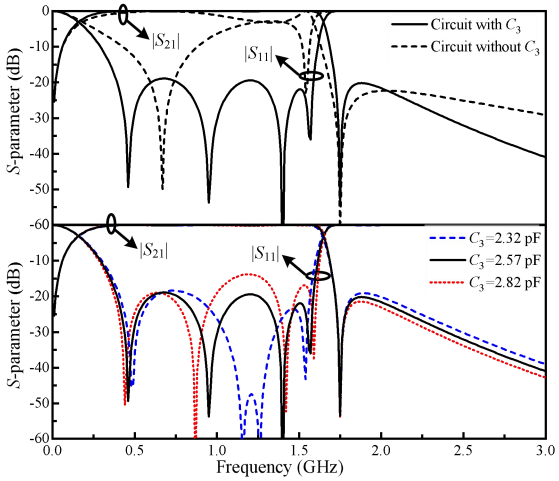

Fig. 2 *The S-parameters with C_3 and without C_3 and the S-parameters of parameter scanning for C_3.*

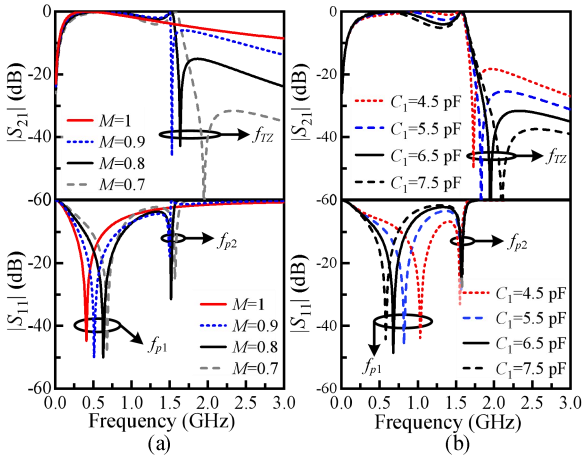

Fig. 3 *(a) The effect of M on the circuit with C_3 removed. (b) The S-parameters of the parameter scanning for C_1.*

matrix of even- and odd-mode equivalent circuits can be obtained, as shown in (1) and (2).

$$A_e = \begin{pmatrix} 1-w^2L_1C_2(M+1) & jwL_1(M+1)(2-w^2L_1C_2(M+1)) \\ jwC_2 & 1-w^2L_1C_2(M+1) \end{pmatrix} \quad (1)$$

$$A_o = \begin{pmatrix} 1+4C_3w^4x_1^2x_2+2(x_2+2C_3)w^2x & -2jwx_1(1+x_1x_2w^2) \\ 8jw((1+x_1x_2w^2)C_3+\frac{x_2}{2})(\frac{1}{2}+w^2x_1C_3) & 1+4C_3w^4x_1^2x_2+2(x_2+2C_3)w^2x_1 \end{pmatrix} \quad (2)$$

where

$$x_1 = (M-1)L_1, x_2 = C_1 + \frac{C_2}{2} \quad (3)$$

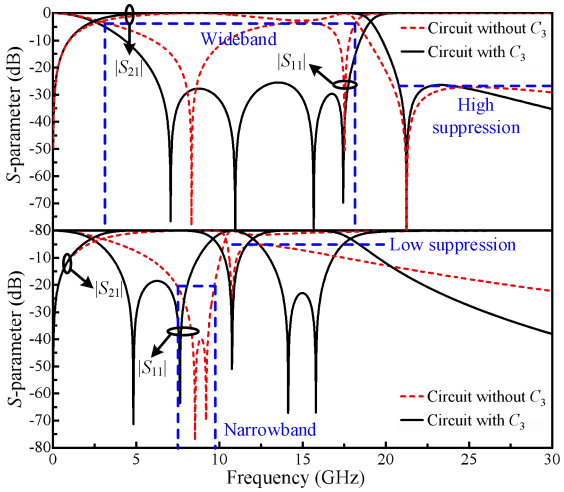

Fig. 4 *The S-parameter of UWB BPF and DBBPF with or without C_3.*

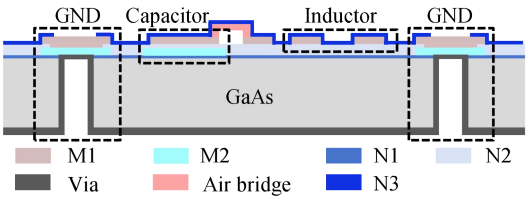

Fig. 5 *The side view of TF-IPD technology.*

According to the method provided in [14], the expression for transmission zero (TZ) is shown in (4). By solving (4), an expression for f_{TZ} can be obtained, as shown in (5). The expression of f_{TZ} reveals its independence from C_3. In addition, when M=1, the expression of f_{TZ} is $f_{TZ}=1/(2\pi L_1C_2)$, and as M decreases, f_{TZ} will move towards higher frequency. In the following, the above characteristics will be combined to further analyze the circuit. Fig.2 shows the S-parameters with C_3 and without C_3 and the S-parameter of parameter scanning for C_3. It can be seen from Fig.2 that f_{TZ} does not change regardless of the presence of C_3 or how C_3 changes. Fig.2 verifies that C_3 does not affect f_{TZ}, so subsequent analysis will remove C_3 from the circuit and then analyze TZ. It is worth noting that when C_3 is removed from the circuit, the four poles of the proposed filter become two.

$$(C_1L_1w^2(M-1)^2+2M-2C_2L_1Mw^2)w=0 \tag{4}$$

$$f_{TZ}=\sqrt{\frac{2M}{L_1(2C_2M-C_1(1-M^2))}} \tag{5}$$

Fig.3 (a) shows the effect of M on the circuit without C_3. With the decrease of M, f_{TZ} will move to the high frequency, which corresponds to the characteristics of (4). It is worth noting that as f_{TZ} moves to the high frequency, f_{p1} and f_{p2} will also move to the high frequency. Fig.3 (b) shows the effect of the change of C_1 on the S-parameter when C_3 is removed. With the increase of C_1, f_{p1} will move to the high frequency greatly, and f_{TZ} and f_{p2} will move to the high frequency slightly.

For the proposed circuit, the resonant frequency of C_2 and L_1 can determine the positions of f_{TZ} and f_{p2}; C_1 and M can both change the positions of f_{p1}, f_{p2}, and f_{TZ}; and the addition of C_3 can increase the two poles.

For UBW BPF, $f_{TZ}=1/(2\pi L_1C_2)$ is set near the upper passband of UBW BPF. By adjusting C_1 and M, the two poles show wideband characteristics and high suppression characteristics after f_{TZ}. The specific curve is shown in Fig.4. When C_3 is added, two additional poles can appear in the passband, and the UWB BPF response can be obtained after debugging. (Component values: C_1=0.41 pF, C_2=0.09 pF, C_3=0.2 pF, L_1=0.99 nH, M=0.67). For DBBPF, $f_{TZ}=1/(2\pi L_1C_2)$ is set near the upper passband of the first passband. By adjusting C_1 and M, the two poles show narrowband characteristics and low suppression characteristics after f_{TZ}. The specific curve is shown in Fig.4. Two additional poles can appear within the second passband when C_3 is added. and the DBBPF response can be obtained after debugging.

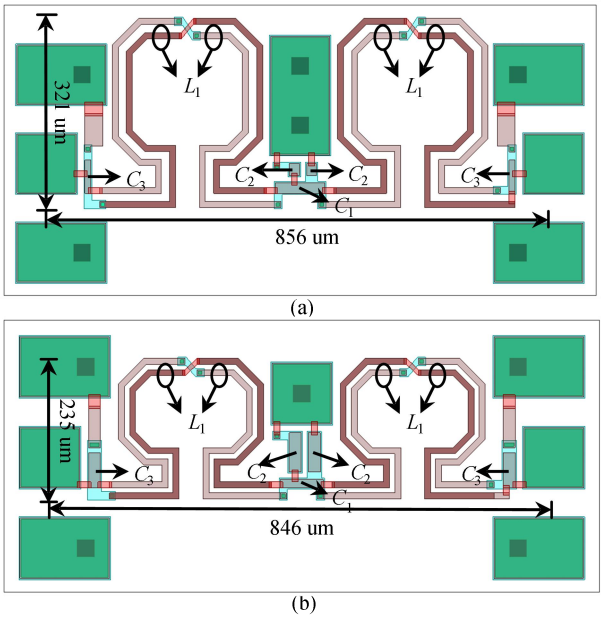

Fig. 6 *(a) The physical structure of UBW BPF. (b) The physical structure of DBBPF.*

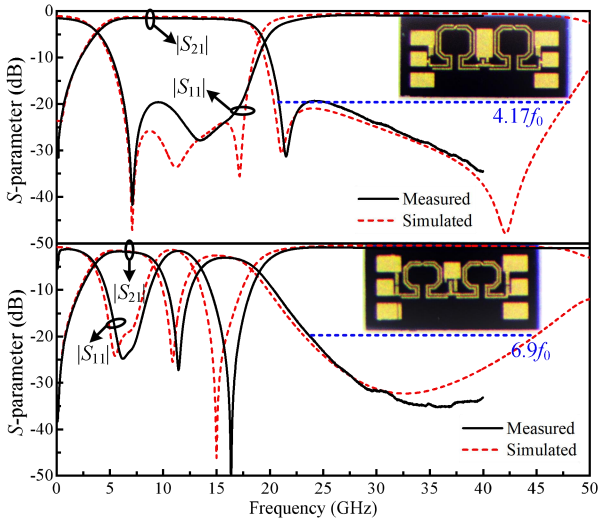

Fig. 7 *The Photographs, simulations, and measurements of UWB BPF and DBBPF.*

(Component values: C_1=0.36 pF, C_2=0.17 pF, C_3=0.36 pF, L_1=0.87 nH, M=0.69).

After the circuit components are determined, the metal-insulator-metal (MIM) capacitor and meander line are used to realize the capacitor and inductor, and the coupling between inductors is realized by the spatial coupling of meander line. Fig.5 shows the TF-IPD technology with a 100 um thick GaAs substrate (dielectric constant of 12.9). Metal layers M1 (thickness of 1 um), M2 (thickness of 3 um), air bridge, and metal on the back of the substrate are formed through gluing, lithography, development, curing, deposition of seed layer and metal evaporation. Dielectric layers N1-N3 are made of SiNx using plasma enhanced chemical vapor deposition (PECVD). N1 layer improves substrate flatness; N2 layer is used as the dielectric for MIM capacitor with a thickness of 0.44 um; N3 layer is a passivation layer that protects the circuit. Fig.6 (a) and (b) exhibit the physical structure of UWB BPF and DBBPF in TF-IPD technology, in sizes of 321 um × 856 um and 235 um × 846 um, respectively (excluding measuring pads).

Experimental results: Fig.7 shows photographs, simulated, and measured results of fabricated UWB BPF and DBBPF. The measured results show that the center frequency of the UWB bandpass filter is 11.43 GHz, with a 3-dB fractional bandwidth of 133% (3.87 GHz-18.99 GHz), a minimum in-band insertion loss of 1.5 dB, and an extended stopband up to 47.7 GHz, and its size is $0.012\lambda_{01}\times0.033\lambda_{01}$ (321 um×

Table I Reference comparison for recent years

	f_c (GHz)	IL (dB)	3-dB FBW (%)	Order	Number*	20-dB rejection	Size (λ_0^2)
[1]	33	1.5	66.7	4	13/10/5	$2.12f_0$	8.47×10^{-4}
[3]	18	2.9	66.7	2	13/12/8	No	4.48×10^{-4}
[4]	26.6	2.6	70	2	11/6/5	NG	5.17×10^{-4}
Pro1	11.43	1.5	133	4	9/5/4	$4.17f_0$	3.96×10^{-4}
[9]	3.32 5.17	1.4 1.5	26 14	4	14/8/5	NG	8.32×10^{-3}
[10]	0.9 2.45	2 1.5	5.46 5.71	4	10/7/4	$5.6f_0$	4.46×10^{-4}
Pro2	6.5 16.2	1.7 3.0	92 35	4	9/5/4	$6.9f_0$	0.9×10^{-4}

Number*: Number of elements/variables/inductors.
Pro1: UWB BPF. Pro2: DBBPF.

856 um), where λ_{01} is the wavelength at 11.43 GHz. And the 3-dB FBWs of DBBPF centered at 6.5 GHz and 16.2 GHz are 92% (3.51-9.49 GHz) and 35% (13.33-18.98 GHz), respectively. The minimum in-band insertion losses are 1.73 dB and 3.04 dB. The stopband of DBBPF can be extended to 44.8 GHz. Its size is $0.005\lambda_{02}\times0.018\lambda_{02}$ (235 um × 846 um), where λ_{02} is the wavelength at 6.5 GHz. Compared with the relevant literature in Table I, the two filters exhibit the characteristics of a simplistic design, miniaturization, and wide stopband.

Conclusion: Based on thin film integrated passive device technology, compact ultra-wideband bandpass filter and dual-band bandpass filter with equal inductance configuration are proposed. The configuration of equal inductance in a circuit contributes to reducing variables, simplifying the physical structure, and shortening the debugging time in the thin film integrated passive device design process. The circuit of both filters is a lumped dual-loop circuit. Although all inductors in the circuit are the same, it can still achieve wide passband. The proposed filters exhibit characteristics such as wideband capability, miniaturization, and wide stopband, making them suitable for integration into communication systems.

Acknowledge: This work was supported by National Natural Science Foundation of China (Grant 62201278), the Natural Science Research Start-up Foundation of Recruiting Talents of Nanjing University of Posts and Telecommunications (Grant NY221120), and Jiangsu Graduate Research Innovation Program (Grant KYCX22_0929).

Corresponding author: Yong Cheng (*The College of Electronic and Optical Engineering & College of Flexible Electronics (Future Technology), Nanjing University of Post and Telecommunications, Nanjing 210046, China.*)
✉ E-mail: chengy@njupt.edu.cn

References

1 L. Gao and G. M. Rebeiz, "Wideband Bandpass Filter for 5G Millimeter-Wave Application in 45-nm CMOS Silicon-on-Insulator", *IEEE Electron Device Lett.*, vol. 42, no. 8, pp. 1244–1247, Aug. 2021.
2 J. Xu, F. Liu, S.-Y. Ji, *et al.*, "An On-Chip Ultra-Wideband Bandpass Filter in 0.18- μ m SiGe BiCMOS Technology", *IEEE Electron Device Lett.*, vol. 43, no. 7, pp. 1009–1012, Jul. 2022.
3 K.-D. Xu, X. Zhu, Y. Yang, *et al.*, "A Broadband On-Chip Bandpass Filter Using Shunt Dual-Layer Meander-Line Resonators", *IEEE Electron Device Lett.*, vol. 41, no. 11, pp. 1617–1620, Nov. 2020.
4 F. Sun, H. Zhu, X. Zhu, *et al.*, "Design of Millimeter-Wave Bandpass Filters With Broad Bandwidth in Si-Based Technology", *IEEE Trans. Electron Devices*, vol. 66, no. 3, pp. 1174–1181, Mar. 2019.
5 Y. Xu, Y. Wu, H. Wu, *et al.*, "Wideband High Selectivity Filter Chips With Adjustable Bandwidth Based on IPD Technology", *IEEE Trans. Circuits Syst. II Express Briefs*, vol. 69, no. 11, pp. 4273–4277, Nov. 2022.
6 Y. Jiang, L. Feng, H. Zhu, *et al.*, "Bandpass Filter With Ultra-Wide Upper Stopband on GaAs IPD Technology", *IEEE Trans. Circuits Syst. II Express Briefs*, vol. 69, no. 2, pp. 389–393, Feb. 2022.
7 D.-M. Kim, B.-W. Min, and J.-M. Yook, "Compact mm-Wave Bandpass Filters Using Silicon Integrated Passive Device Technology", *IEEE Microw. Wirel. Compon. Lett.*, vol. 29, no. 10, pp. 638–640, Oct. 2019.
8 S. Sitaraman, V. Sukumaran, M. R. Pulugurtha, *et al.*, "Miniaturized Bandpass Filters as Ultrathin 3-D IPDs and Embedded Thinfilms in 3-D Glass Modules", *IEEE Trans. Compon. Packag. Manuf. Technol.*, vol. 7, no. 9, pp. 1410–1418, Sep. 2017.
9 L. Hao, Y. Wu, W. Wang, *et al.*, "Design of On-Chip Dual-Band Bandpass Filter Using Lumped Elements in LTCC Technology", *IEEE Trans. Circuits Syst. II Express Briefs*, vol. 69, no. 3, pp. 959–963, Mar. 2022.
10 A. Pourzadi, A. Isapour, and A. Kouki, "Design of Compact Dual-Band LTCC Second-Order Chebyshev Bandpass Filters Using a Direct Synthesis Approach", *IEEE Trans. Microw. Theory Tech.*, vol. 67, no. 4, pp. 1441–1451, Apr. 2019.
11 E. Arabi, M. Lahti, T. Vaha-Heikkila, *et al.*, "A 3-D Miniaturized High Selectivity Bandpass Filter in LTCC Technology", *IEEE Microw. Wirel. Compon. Lett.*, vol. 24, no. 1, pp. 8–10, Jan. 2014.
12 B. Ding, S. Yuan, C. Zhao, *et al.*, "Modeling and Parameter Extraction of CMOS On-Chip Spiral Inductors With Ground Shields", *IEEE Microw. Wirel. Compon. Lett.*, vol. 27, no. 5, pp. 431–433, May 2017.
13 J. Wei and Z. Wang, "Frequency-Independent T Equivalent Circuit for On-Chip Spiral Inductors", *IEEE Electron Device Lett.*, vol. 31, no. 9, pp. 933–935, Sep. 2010.
14 G. I. Zysman and A. K. Johnson, "Coupled Transmission Line Networks in an Inhomogeneous Dielectric Medium", *IEEE Trans. Microw. Theory Tech.*, vol. 17, no. 10, pp. 753–759, Oct. 1969.